JVSTA Journal of Vacuum Science & Technology A

Patterning optically clear films: Coplanar transparent and color-contrasted thin films from interdiffused electrodeposited and solution-processed metal oxides

Colm Glynn, Hugh Geaney, David McNulty, John O'Connell, Justin Holmes, and Colm O'Dwyer

Citation: Journal of Vacuum Science & Technology A **35**, 020602 (2017); doi: 10.1116/1.4968549
View online: http://dx.doi.org/10.1116/1.4968549
View Table of Contents: http://scitation.aip.org/content/avs/journal/jvsta/35/2?ver=pdfcov
Published by the AVS: Science & Technology of Materials, Interfaces, and Processing

Patterning optically clear films: Coplanar transparent and color-contrasted thin films from interdiffused electrodeposited and solution-processed metal oxides

Colm Glynn, Hugh Geaney,[a] David McNulty, and John O'Connell
Department of Chemistry, University College Cork, Cork T12 YN60, Ireland

Justin Holmes
Department of Chemistry, University College Cork, Cork T12 YN60, Ireland; Micro-Nano Systems Centre, Tyndall National Institute, Lee Maltings, Cork T12 R5CP, Ireland; and AMBER@CRANN, Trinity College Dublin, Dublin 2, Ireland

Colm O'Dwyer[b]
Department of Chemistry, University College Cork, Cork T12 YN60, Ireland and Micro-Nano Systems Centre, Tyndall National Institute, Lee Maltings, Cork T12 R5CP, Ireland

(Received 18 October 2016; accepted 8 November 2016; published 28 November 2016)

Transparent thin films can now be site-selectively patterned and positioned on surface using mask-defined electrodeposition of one oxide and overcoating with a different solution-processed oxide, followed by thermal annealing. Annealing allows an interdiffusion process to create a new oxide that is entirely transparent. A primary electrodeposited oxide can be patterned and the secondary oxide coated over the entire substrate to form high color contrast coplanar thin film tertiary oxide. The authors also detail the phase formation and chemical state of the oxide and how the nature of the electrodeposited layer and the overlayer influence the optical clearing of the patterned oxide film. © *2016 American Vacuum Society*.
[http://dx.doi.org/10.1116/1.4968549]

I. INTRODUCTION

The deposition of new and emerging materials for application and incorporation into current and next-generation devices is a significant focus in materials research. The growth in applications of electronics for internet of things (IoT) applications relies on the adaption of current electronic, photonic, and sensor devices with new substrates and materials to form wearable technologies and transparent/flexible devices. Some of these technologies require the development of each aspect of a modern device, including internal electronics, displays, and energy storage/power delivery.[1–7]

At the core of many devices are conductive and dielectric metal oxides. A range of complex oxide materials can be used in the development of next-generation devices and also in displays as the channel materials in transparent or high field-effect mobility thin film transistors (TFTs), which are building blocks for optoelectronic devices.[8–12] The range of applications for new metal oxide materials and structures are desired for different components within modern devices, particularly for thin film electronics and display technologies.[6,13–19] The patterning of different functional layers in modern devices by solution processed methods is under investigation by many groups for application into the (opto)-electronics industry.[15,20–22]

New deposition techniques and methods are required for evolving and innovating deposition of new devices and materials. Deposition techniques range from vapor and physical methods to chemical methods such as solution processing which includes dip-/spin-coating, spray pyrolysis, and screen/ink-jet printing.[6,23–26] Each of these techniques routinely requires postdeposition processing, such as thermal/optical annealing to form the final device layer. Incorporating high transparency is also important, and to do so on any surface at low temperature by interdiffusing two simple oxides to form a complex oxide would be a considerable advance in oxide film growth for scalable and flexible devices and displays. A solid-state interdiffusion technique that utilizes solution processing methods and low temperature annealing for the formation of complex oxide materials has been previously demonstrated for V-O-Na-Si materials.[27,28] The benefit of the interdiffusion technique lies in the solid-state formation of the material after the initial deposition of a metal oxide thin film without requiring extra wet chemical processing.

Here, we detail a technique for creating patterned films of a transparent oxide thin film material by thermal interdiffusion of Si and Na species from patterned electrodeposited Na-containing SiO_2, underneath a solution-processed vanadium oxide (VO) thin film overlayer. Electrodeposition of SiO_2 that provides mobile silica species for interdiffusion, in addition to Na from the electrolyte, allows optical clearing of overlapping regions on patterned conductive substrates such as fluorine-doped tin oxide (FTO). The findings show how Na from the electrolyte affects SiO_2 electrodeposition and that the codiffusion of both species from overcoated oxide films during the interdiffusion process with VO facilitates optical transparency in thin films, and the formation of coplanar templated or patterned regions with strong optical contrast.

[a]Present address: Materials and Surface Science Institute, University of Limerick, Limerick, Ireland.
[b]Author to whom correspondence should be addressed; electronic mail: c.odwyer@ucc.ie

II. EXPERIMENT

A. Thin film formation and processing

SiO_2 thin films were prepared using a modified electrodeposition technique.[29] The electrodeposition electrolyte was prepared by mixing and stirring 40 ml EtOH with 6 ml tetraethyl orthosilicate (TEOS) for 3 h with 40 ml of a 0.1 M Sodium Nitrate ($NaNO_3$) and 10^{-3} M hydrochloric acid (HCl) aqueous solution. A second electrodeposition electrolyte was prepared without the $NaNO_3$ salt in order to deposit pure SiO_2 films without Na species.

Electrodeposition was performed on 350 nm thick FTO coated glass substrate working electrode with a platinum mesh counter electrode and saturated calomel reference electrode. Electrodeposition was performed at a constant potential of −2.5 V for 10 s on a Princeton Applied Research VersaSTAT 3 potentiostat. Templated depositions were prepared using custom 3D printed stencils built using a MakerBot Replicator 2X system from acrylonitrile butadiene styrene plastic. Plastic 3D printed templates were secured to the front of the FTO to ensure electrical contact to the electrolyte with only the uncovered substrate surface.

V-O-Na-Si and V-O-Si thin films were formed by dip-coating an amorphous VO layer onto the electrodeposited SiO_2 thin films from a vanadium triisopropoxide, iso-propyl alcohol (IPA), and H_2O based precursor solution at a mixture by volume of 1000:10:1 (IPA:Alkoxide:H_2O). Dip-coating was performed on a PTL-MM01 desktop dip coater at a constant withdraw rate of 2.5 mm/s and repeated three times for each coating. Subsequent thermal anneals were performed in a conventional oven at 300 °C to facilitate the interdiffusion processes between the VO and SiO_2 films.

B. Analysis techniques

The surface morphology was examined with an FEI Quanta 650 FEG high resolution SEM with operating voltages of 10–20 kV. Raman scattering spectroscopy was collected on a Renishaw InVia Raman spectrometer using a 514 nm 30 mW laser source. Spectra were collected and focused onto the samples using a 50 × objective lens. X-ray photoelectron spectroscopy (XPS) spectra were acquired on an Oxford Applied Research Escabase XPS system equipped with a CLASS VM 100 mm mean radius hemispherical electron energy analyzer with multichannel detectors in an analysis chamber with a base pressure of 3.0×10^{-9} mbar. A nonmonochromated Al-Kα x-ray source at 150 W was used for all scans.

III. RESULTS AND DISCUSSION

The formation of SiO_2 thin films on a range of substrates can be accomplished by electrodeposition using TEOS. The generation of OH^- groups at the working electrode substrate surface in a three-electrode electrochemical cell facilitates hydrolysis and polycondensation reactions depositing a solid film of SiO_2 material.[29–33] The SiO_2 film is subsequently dip-coated with an overlayer of amorphous VO, and after subsequent thermal annealing at 300 °C, a V-O-Na-Si phase material is formed through solid-state interdiffusion processes. The optical images in Fig. 1(a) show an as-deposited and thermally annealed SiO_2 and V-O-Na-Si film, respectively. For ease of identification of the films, their colors and the optical clearing from thermal interdiffusion, half an electrodeposited SiO_2 thin film (containing O-Na-Si) was overcoated with VO to form a staggered SiO_2/VO bi-layered deposit. The schematic of Fig. 1(a) outlines

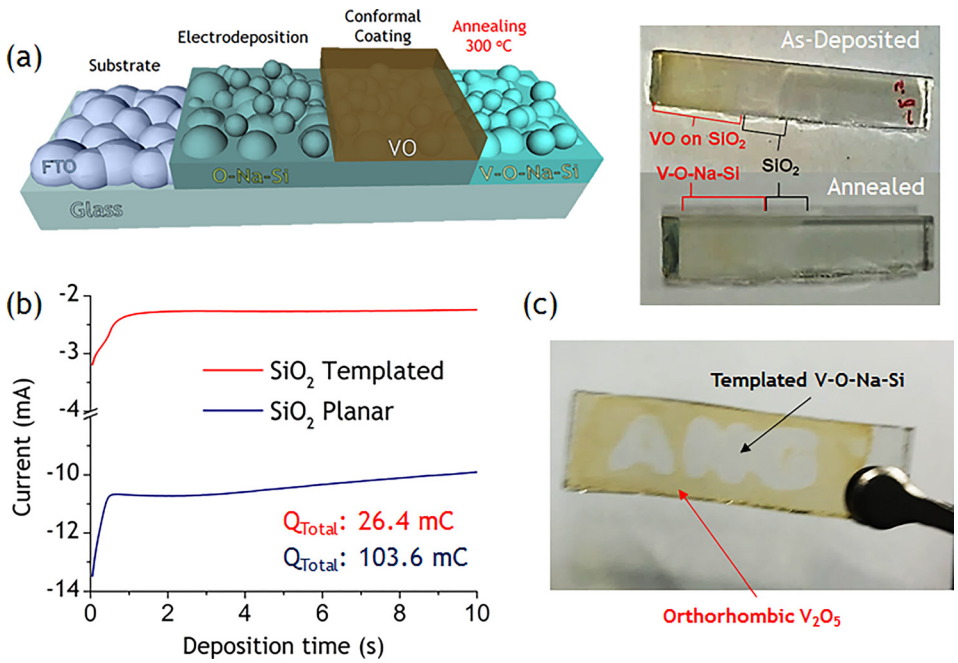

FIG. 1. (Color online) (a) Schematic illustrates the formation of V-O-Na-Si through thermal annealing of dip-coated VO on electrodeposited SiO_2 films. Optical images of the electrodeposited SiO_2, VO coated SiO_2 (top), and thermally annealed SiO_2 and V-O-Na-Si (bottom). (b) $I(t)$ profile for planar and templated electrodeposition of SiO_2 on FTO at an applied voltage of −2.5 V. (c) Optical image of templated V-O-Na-Si surrounded by orthorhombic V_2O_5.

the processes in the formation of a V-O-Na-Si film through the interdiffusion processes.

Planar electrodeposition of SiO_2 on FTO substrates was carried out by chronoamperometry at an applied voltage of −2.5 V for 10 s, shown in Fig. 1(b). After an initial rapid change in current from nucleation of the electrodeposited layer, the reaction rate (current) levels to a consistent growth rate (as measured by the cumulative charge passed) increases slightly. Film growth thus increases roughly linearly in time (further analysis is provided in supplementary material Sec. II).[44] The total charge (Q_{Total}) for deposition at −2.5 V for 10 s is 103.6 mC. After thermal annealing, the interdiffusion between the VO and O-Na-Si forms a fully transparent V-O-Na-Si mixed material where the O-Na-Si interdiffused with the VO, which optically clears both the white color of the SiO_2 and the yellow color of the VO. An optical image of a templated SiO_2 electrodeposition coated with VO to form the V_2O_5/V-O-Na-Si template after thermal annealing is shown in Fig. 1(c).

SEM analysis of the electrodeposited SiO_2, the as-deposited VO-coated SiO_2, and thermally annealed V-O-Na-Si is presented in supplementary material Sec. I. The electrodeposited SiO_2 has a thickness of ∼500–800 nm with a surface morphology composed of spherical particles on top of a denser SiO_2 film. The dip-coated VO conformally coats the SiO_2 surface with an average thickness of ∼15 nm per dip-coated layer to a maximum total thickness of ∼45–50 nm (three layers).[27,34] After thermal annealing and interdiffusion process that forms the V-O-Na-Si material, the film surface roughens with an increase in porosity evident in supplementary material Figs. S1 and S2.

In this work, two types of electrodeposited SiO_2 planar thin films are grown onto which solution processed VO is dip-coated. In the first type, a mixed Na and SiO_2 material mixture is electrodeposited, where Na was added to the TEOS-based electrolyte with a $NaNO_3$ salt additive. The second type of planar electrodeposited SiO_2 film contains only O and Si species, without any $NaNO_3$ electrolyte additive. Previous publications have discussed the role of Na species in the interdiffusion formation of $NaVO_3$ materials.[27,28] The role of Si interdiffusion from the SiO_2 into the VO was directly examined and compared by removing the Na species from the electrolyte. The electrodeposition of SiO_2 (O-Na-Si) and SiO_2 (without Na^+) and subsequent VO coating and interdiffusion, forming V-O-Si, is examined in detail in supplementary material Sec. II.

The Raman spectra for FTO, electrodeposited SiO_2, electrodeposited SiO_2 (no $NaNO_3$ additive), thermally annealed V-O-Si, orthorhombic V_2O_5 thin film and thermally annealed V-O-Na-Si regions are shown in Fig. 2(a). The characteristic vibrational modes in the annealed transparent V-O-Na-Si corresponds to the presence of α-$NaVO_3$, with the most prominent high wavenumber modes at 918 and 953 cm^{-1}, respectively.[27] After thermal annealing and the formation of V-O-Si (SiO_2 without Na^+), the Raman scattering spectrum does not show the characteristic phonon modes for orthorhombic V_2O_5, nor $NaVO_3$ modes, which would be expected on the surface after annealing without

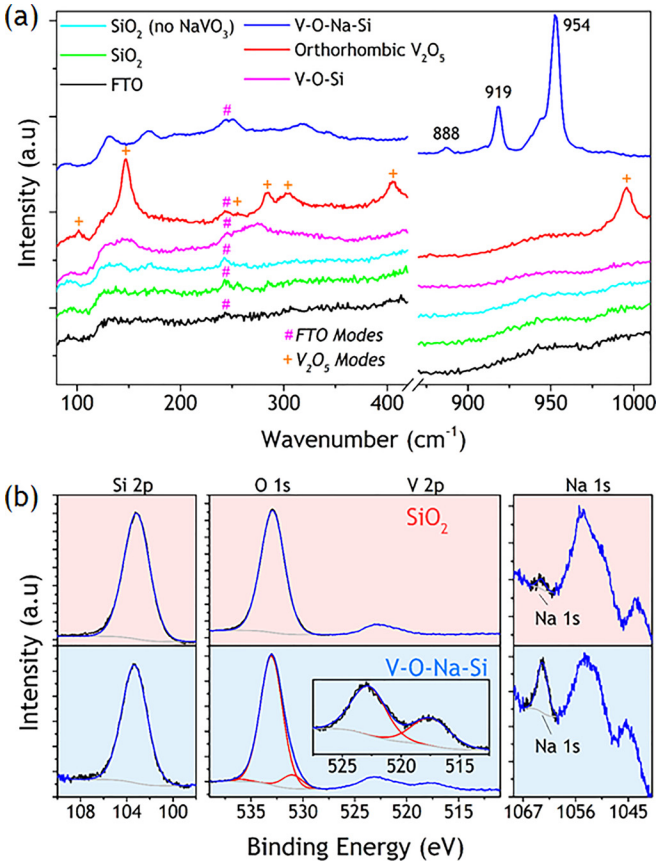

FIG. 2. (Color online) (a) Raman scattering spectroscopy of FTO, electrodeposited SiO_2, electrodeposited SiO_2 (no $NaNO_3$ additive), thermally annealed V-O-Si, orthorhombic V_2O_5 thin film, and thermally annealed V-O-Na-Si. The vibrational modes characteristic to FTO and orthorhombic V_2O_5 are highlighted. (b) XPS spectrum for the SiO_2 and V-O-Na-Si thin films showing the binding energies for the Si 2p, O 1s, V 2p, and Na 1s core-levels. The Auger peaks for SnO_2 and Sn are located at ∼1055 and 1046 eV, respectively, and are attributed to areas of the FTO substrate visible to the x-ray spot.

interdiffusion. Only the V-O-Na-Si formation from interdiffusion of both films results in complete optical clearing of the white Na-containing SiO_2 and yellow VO thin film colors. As the formation of orthorhombic V_2O_5 is not found after annealing the bilayer of the Na-free electrodeposited SiO_2 coated in VO, interdiffusion between the Si, V, and O species must form an amorphous, non-Raman active material. This provides proof that the interdiffusion process is not limited to V and Na species, but the latter are always required to form the optically transparent $NaVO_3$ constituent.

To examine the composition of the optically cleared V-O-Na-Si film compared to the individual electrodeposited and solution-processed SiO_2 and VO thin films, XPS of the Si 2p, O 1s, V 2p, Na 2p, and Na 1s core-levels are presented in Fig. 2(b). We observe no change to the Si 2p photoemission at 103.2 eV after the formation of the V-O-Na-Si material, which is to be expected due to the large amount of SiO_2 present and low concentration of VO deposited on the surface; SiO_2 remains in its original chemical state. The O 1s peak has an extra shoulder contribution at 530.9 eV, which is attributed to the formation of α-$NaVO_3$ on the surface by interdiffusion of the Na cations. The V 2p peak is located at

517.7 eV and correlates to the binding energy for V in $NaVO_3$.[35] Interestingly, the Na 1s increases in intensity after the interdiffusion process occurs. The higher quantity of Na 1s in the vicinity of the surface is attributed to the diffusion of Na^+ from within the electrodeposited SiO_2 film to the surface during the formation of the V-O-Na-Si material. While the final phase is a mixed crystalline $NaVO_3$ component together with an Si-O containing glassy matrix, the relative stoichiometry from atomic percent of the final phase at the surface of the V-O-Si-Na is V (2.54%)-O (60.76%)-Si (0.55%)-Na (36.15%).

Surface composition analysis using the XPS survey spectrum shows that the surface prior to VO deposition is composed of 3% Na, 38.25% Si, and 58.75% O. Assuming that areas of the FTO substrate is in view of the x-ray beam [allowing Sn and SnO_2 Auger peaks in Fig. 2(b) to be seen], the contribution of the bonded O species for FTO increases the percentage of O in the composition calculation. As the Si 2p peak is referenced to SiO_2, the assumption that Na species is deposited within the SiO_2 material leads to an estimation of the electrodeposited material to be $Na_{0.1}SiO_2$. After dip-coating an overlayer of VO and subsequent annealing, the Na species within the $Na_{0.1}SiO_2$ thin film interdiffuses with the VO forming the V-O-Na-Si, in which the α-$NaVO_3$ crystalline material forms.

Patterned substrates and thin films are used in a range of applications from electronic devices,[36] optical coatings,[37–39] sensors,[20] and batteries.[38] A range of methods are available for the deposition of patterned and structured substrates/thin films. Techniques for altering the surface chemistries in solution-processed techniques, where alterations are made to the wettability of surfaces, can be employed for the preparation of patterns such as stripes, lines, and single deposits.[21,40–42] The formation of interdigitated circuits and electrodes of multiple or complex oxide phases may also be beneficial for high- or low-k electronic materials, absorption-tuned photoanodes, electrochromics, sensors, or TFT dielectric or channel materials.[20,43] Directly forming transparent or color-contrasted materials in the same film coating for these applications provides a simple way of templating or patterning optically clear regions of coating coplanar with the original films, and for high optical contrast/conductivity patterns across large substrate areas.

To demonstrate this possibility, we used custom 3D-printed template masks during electrodeposition to form templated SiO_2 thin film structures. By dip-coating this substrate with VO thin films and annealing the overall deposit, a patterned transparent V-O-Na-Si thin film surrounded by coplanar yellow-colored orthorhombic V_2O_5 is formed, forming an in-plane heterojunction of conducting and non-conducting oxides with significantly different degrees of optical transparency. Macrosized templates were prepared in order to demonstrate the concept, whereby a combination of electrodeposition and interdiffusion processes can form

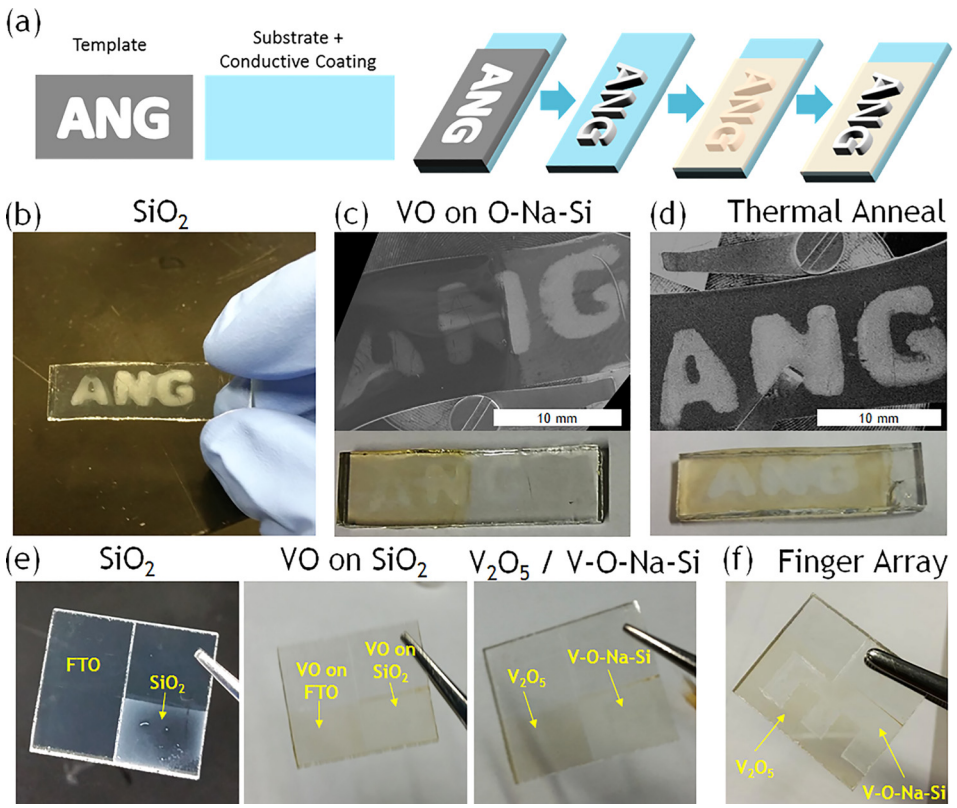

FIG. 3. (Color online) (a) Schematic detailing the deposition of templated V-O-Na-Si through electrodeposition of SiO_2, VO coating and subsequent thermal annealing. Optical image of (b) templated SiO_2 on FTO. Optical and SEM images of (c) templated SiO_2 half coated in VO prior to thermal annealing and (d) formation of V-O-Na-Si material surrounded by an orthorhombic V_2O_5 thin film after thermal annealing. [(e) and (f)] Optical images of possible interdigitated V_2O_5/V-O-Na-Si depositions on FTO with a simple planar and finger array, respectively.

patterned transparent features of films and materials on substrates.

The electrodeposition $I(t)$ profile for a templated SiO_2 deposition compared to that of a planar SiO_2 deposition was shown in Fig. 1(b). The templated deposition has a lower initial current with a noticeable change in the profile shape between the two depositions from 0.3 to 2 s. The decrease in total charge passed (from 103.6 to 26.4 mC) is attributed to a reduction in available surface area for the electrodeposition in the template. A schematic of the procedure for depositing the templated SiO_2, VO on SiO_2 and V-O-Na-Si samples is shown in Fig. 3(a). A 3D printed template was placed on the bare FTO and SiO_2 electrodeposition formed a thin film matching the templated area. The entire substrate was then iteratively dip-coated with VO (covering the FTO and SiO_2) and thermally annealed. Optical and SEM images of the templated SiO_2, VO on SiO_2, and thermally annealed V-O-Na-Si are shown in Figs. 3(b)–3(d), respectively, including half-coated samples to demonstrate the optical clearing from the overlapping deposit regions where interdiffusion occurs [Fig. 3(c)]. The templated as-deposited SiO_2 thin films are optically opaque. After VO dip-coating, thermal annealing results in subsequent interdiffusion and oxide phase conversion. The nontemplated regions form yellow-colored crystalline orthorhombic V_2O_5 while the formation of transparent V-O-Na-Si occurs uniquely on the templated SiO_2 coated by VO. In Figs. 3(e) and 3(f) other examples of templated depositions featuring planar and finger array patterns are shown to demonstrate the versatility of coplanar patterned optical absorbance contrast in the same thin film.

In-depth SEM and Raman scattering spectroscopy analysis for the templated SiO_2 and V-O-Na-Si coatings is shown in supplementary material Sec. III. The SEM images of the templated SiO_2 a show a lower surface roughness compared to planar deposits discussed above, but the dip-coated VO on the templated SiO_2 is rougher compared to the conformal coatings formed on nontemplated planar deposits. This nonconformal coating is attributed to the change in the morphology of the templated electrodeposited SiO_2 (see supplementary material Sec. III). After thermal annealing, however, the templated surface retains a high roughness, although as shown in Fig. 3(d) complete optical clearing still occurs confirming the interdiffusion process is efficient and possible on smooth and rough bilayered coatings. The Raman scattering spectra for the films show the formation of orthorhombic V_2O_5 on the FTO regions surrounding the templated SiO_2 regions.

IV. SUMMARY AND CONCLUSIONS

Using 3D printed shadow mask-type templates to pattern the electrodeposited layer (or indeed optical lithography could be used), the subsequent overcoat of the entire substrate with the VO results in coplanar color-contrasted patterned thin films. Interdiffusion in this case forms V-O-Na-Si materials which is optically cleared and exhibits well defined in-plane interfaces and surface areas with no stitching defects (as the entire surface of patterned and unpatterned regions are covered in the overlayer oxide). A single thermal annealing step resulted in the formation of a distinct orthorhombic V_2O_5/V-O-Na-Si patterned substrate.

Interdiffusion processes that modify predeposited coatings, that do not detrimentally alter the initial surface should be very useful for applications in nanoelectronics, sensors, (photo)electrochemical anodes/cathodes, and indeed for transparent optical/optoelectronic devices where tight constraints on surface defects and transparency are required from solution-processing. Electrodeposition coupled with dip-coating makes the method versatile and scalable, with lithographic patterning providing routes to pattern and define high color contrast coatings at much lower temperatures than many physical deposition methods. The interdiffusion process may in future be useful for the localized phase conversion of complex oxide materials, dielectric or channel thin films and provide for oxide coverage of substrates in planar of coplanar form with contrasting optical absorbance using separately deposited simple oxides.

ACKNOWLEDGMENTS

C.G. acknowledges the support of the Irish Research Council under Award No. RS/2011/797. The authors acknowledge support from the Irish Research Council New Foundations Award. This work was also supported by Science Foundation Ireland (SFI) under the National Access Programme (NAP 417), and through SFI Technology Innovation and Development Awards 2013 and 2015 under Contract Nos. 13/TIDA/E2761 and 15/TIDA/2893.

[1]K. Myny *et al.*, Sci. Rep. **4**, 7398 (2014).
[2]J.-S. Park *et al.*, Appl. Phys. Lett. **95**, 013503 (2009).
[3]A. M. Gaikwad, A. C. Arias, and D. A. Steingart, Energy Technol. **3**, 305 (2015).
[4]A. M. Gaikwad, B. V. Khau, G. Davies, B. Hertzberg, D. A. Steingart, and A. C. Arias, Adv. Energy Mater. **5**, 1401389 (2015).
[5]J. Leppaniemi, O. H. Huttunen, H. Majumdar, and A. Alastalo, Adv. Mater. **27**, 7168 (2015).
[6]C. Glynn and C. O'Dwyer, "Solution processable metal oxide thin film deposition and material growth for electronic and photonic devices," Adv. Mater. Interf. (unpublished).
[7]L. Petti, N. Munzenrieder, C. Vogt, H. Faber, L. Buthe, G. Cantarella, F. Bottacchi, T. D. Anthopoulos, and G. Troster, Appl. Phys. Rev. **3**, 021303 (2016).
[8]J. Jiang, Y. Li, J. Liu, X. Huang, C. Yuan, and X. W. Lou, Adv. Mater. **24**, 5166 (2012).
[9]H.-J. Freund and G. Pacchioni, Chem. Soc. Rev. **37**, 2224 (2008).
[10]C.-C. Chueh, C.-Z. Li, and A. K. Y. Jen, Energy Environ. Sci. **8**, 1160 (2015).
[11]J. H. Park, J. Y. Oh, S. W. Han, T. I. Lee, and H. K. Baik, ACS Appl. Mater. Interfaces **7**, 4494 (2015).
[12]X. Yu, T. J. Marks, and A. Facchetti, Nat. Mater. **15**, 383 (2016).
[13]K. Si Joon, Y. Seokhyun, and K. Hyun Jae, Jpn. J. Appl. Phys., Part 1 **53**, 02BA02 (2014).
[14]D. H. Lee, Y. J. Chang, G. S. Herman, and C. H. Chang, Adv. Mater. **19**, 843 (2007).
[15]W.-J. Lee, W.-T. Park, S. Park, S. Sung, Y.-Y. Noh, and M.-H. Yoon, Adv. Mater. **27**, 5043 (2015).
[16]Q. Jiang, L. Feng, C. Wu, R. Sun, X. Li, B. Lu, Z. Ye, and J. Lu, Appl. Phys. Lett. **106**, 053503 (2015).
[17]S. R. Thomas, P. Pattanasattayavong, and T. D. Anthopoulos, Chem. Soc. Rev. **42**, 6910 (2013).
[18]A. Grill, S. M. Gates, T. E. Ryan, S. V. Nguyen, and D. Priyadarshini, Appl. Phys. Rev. **1**, 011306 (2014).

[19]A. O. Cetinkaya, S. Kaya, A. Aktag, E. Budak, and E. Yilmaz, Thin Solid Films **590**, 7 (2015).
[20]N. Shirahata, W. Shin, N. Murayama, A. Hozumi, Y. Yokogawa, T. Kameyama, Y. Masuda, and K. Koumoto, Adv. Funct. Mater. **14**, 580 (2004).
[21]Y. Wang and T. J. McCarthy, Langmuir **30**, 2419 (2014).
[22]Y. Masuda and K. Koumoto, U.S. patent 8,715,811 B2 (6 May 2014).
[23]T. Schneller, R. Waser, M. Kosec, and D. Payne, *Chemical Solution Deposition of Functional Oxide Thin Films*, 1st ed. (Springer, London, 2013).
[24]H. Kakiuchi, H. Ohmi, and K. Yasutake, J. Vac. Sci. Technol., A **32**, 030801 (2014).
[25]P. K. Nayak, J. A. Caraveo-Frescas, Z. Wang, M. N. Hedhili, Q. X. Wang, and H. N. Alshareef, Sci. Rep. **4**, 4672 (2014).
[26]F. Nicholas, M. P. Sean, W. H. Mark, and S. S. N. Bharadwaja, J. Phys. D: Appl. Phys. **42**, 055408 (2009).
[27]C. Glynn, D. Aureau, G. Collins, S. O'Hanlon, A. Etcheberry, and C. O'Dwyer, Nanoscale **7**, 20227 (2015).
[28]C. Glynn, D. McNulty, H. Geaney, and C. O' Dwyer, Small **12**, 5954 (2016).
[29]A. Walcarius, E. Sibottier, M. Etienne, and J. Ghanbaja, Nat. Mater. **6**, 602 (2007).
[30]S. Sayen and A. Walcarius, Electrochem. Commun. **5**, 341 (2003).
[31]E. Sibottier, S. Sayen, F. Gaboriaud, and A. Walcarius, Langmuir **22**, 8366 (2006).
[32]A. Walcarius and E. Sibottier, Electroanalysis **17**, 1716 (2005).
[33]M. M. Collinson, D. A. Higgins, R. Kommidi, and D. Campbell-Rance, Anal. Chem. **80**, 651 (2008).
[34]C. Glynn, D. Creedon, H. Geaney, E. Armstrong, T. Collins, M. A. Morris, and C. O'Dwyer, Sci. Rep. **5**, 11574 (2015).
[35]P. Mezentzeff, Y. Lifshitz, and J. W. Rabalais, Nucl. Instrum. Methods Phys. Res. Sec. **44**, 296 (1990).
[36]S. Hoeppener, R. Maoz, and J. Sagiv, Nano Lett. **3**, 761 (2003).
[37]W. Niu, L. T. Su, R. Chen, H. Chen, Y. Wang, A. Palaniappan, H. Sun, and A. I. Yoong Tok, Nanoscale **6**, 817 (2014).
[38]E. Armstrong and C. O'Dwyer, J. Mater. Chem. C **3**, 6109 (2015).
[39]J. Liao, Z. Yang, H. Wu, D. Yan, J. Qiu, Z. Song, Y. Yang, D. Zhou, and Z. Yin, J. Mater. Chem. C **1**, 6541 (2013).
[40]D. Tian, Y. Song, and L. Jiang, Chem. Soc. Rev. **42**, 5184 (2013).
[41]D. Noguera-Marín, C. L. Moraila-Martínez, M. A. Cabrerizo-Vílchez, and M. A. Rodríguez-Valverde, Langmuir **30**, 7609 (2014).
[42]T. P. Corrales *et al.*, ACS Nano **8**, 9954 (2014).
[43]J. H. Pikul, H. Gang Zhang, J. Cho, P. V. Braun, and W. P. King, Nat. Commun. **4**, 1732 (2013).
[44]See supplementary material at http://dx.doi.org/10.1116/1.4968549 for full SiO_2 and V-O-Na-Si surface morphology analysis, and further characterization data from electrodeposition and templated deposits.